De-Shadowing of Satellite/Airborne Multispectral and Hyperspectral Imagery

R. Richter
DLR, German Aerospace Center
Remote Sensing Data Center
D-82234 Wessling
GERMANY

ABSTRACT

A de-shadowing technique is presented for multispectral and hyperspectral imagery over land acquired by satellite / airborne sensors. The method requires a channel in the visible and at least one spectral band in the near-infrared (0.8-1 µm) region, but performs much better if bands in the short-wave infrared region (around 1.6 and 2.2 µm) are available as well. Five major processing steps are employed : (1) the calculation of the covariance matrix and zero-reflectance matched filter vector based on atmospherically corrected surface reflectance data, (2) the derivation of the unscaled and scaled shadow function, (3) a histogram thresholding of the unscaled shadow function to define the core shadow areas, (4) a region growing to include the surroundings of the core shadow areas for a smooth shadow/clear transition, and (5) the de-shadowing of the pixels in the final shadow mask using the scaled shadow function. A radiative transfer code is employed in the last step to compute the de-shadowed surface reflectance imagery. Example images of hyperspectral airborne and multispectral spaceborne are presented.

1. INTRODUCTION

Remotely sensed optical imagery of the Earth's surface is often contaminated with cloud and cloud shadow areas. Surface information under cloud covered regions cannot be retrieved with optical sensors, because the signal contains no ground component. In shadow areas, however, the ground-reflected solar radiance is always a small non-zero signal, because the total radiation signal at the sensor contains a direct (beam) and a diffuse (reflected skylight) component. Even if the direct solar beam is completely blocked in shadow regions, the reflected diffuse flux will remain. Therefore, an estimate of the fraction of direct solar irradiance for a fully or partially shadowed pixel can be the basis of a compensation process called de-shadowing or shadow removal.

Several de-shadowing techniques have been described in the literature. One approach employs geometric considerations to project the cloud structure on the ground based on the direction of the incident solar radiation and the estimated cloud height (Simpson and Stitt 1998). Another approach uses the matched filter concept (Adler-Golden et al. 2002) where the matched filter vector is calculated in terms of the covariance matrix of the atmospherically corrected reflectance data.

This contribution also employs the matched filter concept as one step of the de-shadowing method. The application of the matched filter vector to the atmospherically corrected reflectance imagery yields unscaled, positive and negative shadow abundance values. However, the re-scaling of the unscaled function into the physical interval (0,1), containing the fraction of direct illumination, is performed with a new strategy, as detailed in the next section.

Richter, R. (2005) De-Shadowing of Satellite/Airborne Multispectral and Hyperspectral Imagery. In *Emerging EO Phenomenology* (pp. 5-1 – 5-8). Meeting Proceedings RTO-MP-SET-094, Paper 5. Neuilly-sur-Seine, France: RTO. Available from: http://www.rto.nato.int/abstracts.asp.

All mentioned spectral methods imply the linear independence of pure spectra. This may not be true, especially in complex scenes. So mis-classifications do occur. As an example, a fully illuminated pixel of a dark material can be classified as a shadowed pixel of another material or combination of materials. Still, useful de-shadowed images have been processed for a variety of different climatic and landscape conditions.

2. DE-SHADOWING METHOD

The method consists of a sequence of processing steps, see Fig. 1. It starts with a calculation of the surface reflectance image cube $\rho_i = \rho(\lambda_i)$, where three spectral bands around λ_i = 0.85, 1.6, and 2.2 µm are selected. These bands from the near and shortwave infrared region are very sensitive to cloud shadow effects, because the direct part of the solar radiation flux at the ground level is typically 80% or more of the total downwelling flux, see Fig. 2. Channels in the blue-to-red region (0.4 - 0.7 µm) are not used for the detection of shadow regions because they receive a much larger diffuse radiation component, making them less sensitive to partial shadow effects. In this contribution the ATCOR code is used for the atmospheric correction (Richter 1996, 1998, Richter and Schläpfer 2002, http://www.rese.ch), which employs a database of radiative transfer calculations based upon MODTRAN (Berk et al., 2000).

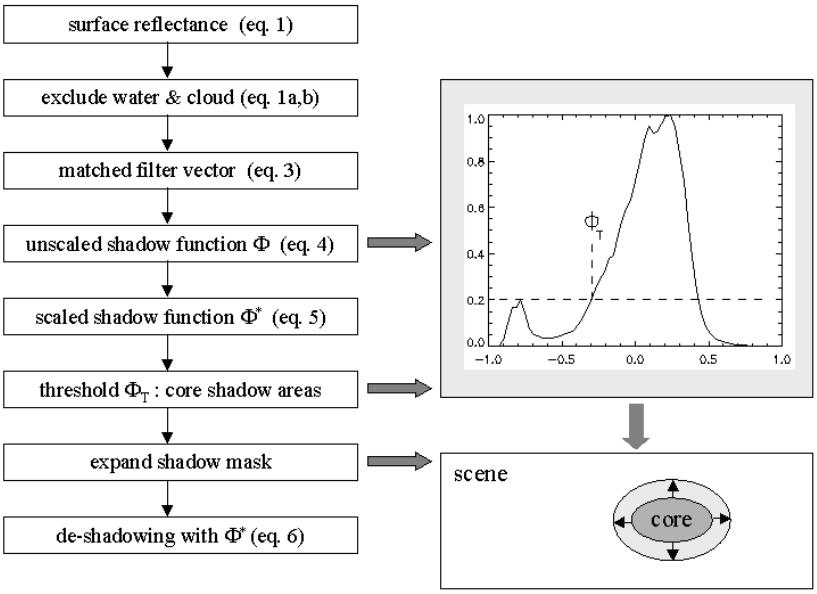

Fig. 1: Processing steps of de-shadowing method.

The surface reflectance is first computed with the assumption of full solar illumination, i.e., the global flux on the ground consists of the direct (E_{dir}) and diffuse (E_{dif}) component. If DN denotes the digital number of a pixel, L_P the path radiance, and τ the atmospheric transmittance (ground-to-sensor) the surface reflectance can be obtained as (Richter 1996) :

$$\rho_i(x,y) = \frac{\pi \left(d^2 \left\{ c_0(i) + c_1(i) DN_i(x,y) \right\} - L_{p,i} \right)}{\tau_i \left(E_{dir,i} + E_{dif,i} \right)} \qquad (1)$$

Here, d is the Earth-Sun distance at the image acqusition time in astronomical units, c_0 and c_1 are the radiometric calibration coefficients (offset and slope) to convert the digital number into the corresponding at-sensor radiance L, i.e., $L = c_0 + c_1$ DN , and i is the channel index.

The next step is the masking of water bodies and cloud areas with simple spectral criteria as detailed in the following discussion section. Water pixels have to be excluded as far as possible to avoid their assignment as shadow pixels. In addition, cloud pixels should not be processed. This is achieved with the following thresholds:

$\rho(0.48\ \mu m) \geq 30\ \%$ and $\rho(1.6\ \mu m) \geq 30\ \%$ (cloud) (1a)

$\rho(0.85\ \mu m) \leq 5\%$ and $\rho(1.6\ \mu m) \leq 1\ \%$ (water) (1b)

Step 3 calculates the covariance matrix $C(\rho')$ where ρ' is the reflectance vector comprising only the non-water and non-cloud pixels. For each pixel, this vector holds the reflectance values in the 3 selected channels (around 0.85, 1.6, 2.2 µm). The matched filter is a vector tuned to a certain target reflectance spectrum ρ'_t to be detected (Adler-Golden et al. 2002) :

$$V_{mf} = -\frac{C^{-1}(\rho'_t - \overline{\rho}')}{(\rho'_t - \overline{\rho}')^T C^{-1}(\rho'_t - \overline{\rho}')} \tag{2}$$

Here, $\overline{\rho}'$ is the scene-average spectrum, without the water/cloud pixels. Selecting $\rho'_t = 0$ for a shadow target yields a special simplified form of the matched filter, where the 'sh' index symbolizes shadow :

$$V_{sh} = -\frac{C^{-1}\,\overline{\rho}'}{\overline{\rho}'^T C^{-1}\overline{\rho}'} \tag{3}$$

The shadow matched filter vector is then applied to the non-water/non-cloud part of the scene and yields the still un-normalized values Φ that are a relative measure of the fractional direct illumination, also called *unscaled shadow function* here :

$$\Phi(x,y) = V_{sh}^T\left(\rho'(x,y) - \overline{\rho}'\right) \tag{4}$$

The matched filter calculates a minimum RMS shadow target abundance for the entire (non-water/non-cloud) scene. Therefore, the values of Φ are positive and negative numbers.

The arbitrary, image-depending range of Φ has to be rescaled to the physical range from 0 to 1, where 0 indicates no direct illumination (full shadow), and 1 means full direct illumination. The histogram of Φ is used to rescale the data. For this purpose, we assume that the location of the main peak at Φ_{max} represents fully illuminated areas. It is based on the statistical reasoning that full direct solar illumination is already obtained for surfaces of average scene brightness. Then the values Φ are linearly mapped from the unscaled (Φ_{min}, Φ_{max}) interval onto the physically scaled (0,1) interval, where the *scaled shadow function* is named Φ^* :

$$\Phi^* = \frac{\Phi - \Phi_{min}}{\Phi_{max} - \Phi_{min}} \quad \text{if} \quad \Phi \leq \Phi_{max} \tag{5a}$$

$$\Phi^* = 1 \quad \text{if} \quad \Phi > \Phi_{max} \tag{5b}$$

The smallest value of the scaled shadow function is $\Phi^*_{min} = 0$, which means no direct illumination. However, to avoid overcorrection and to cope with scenes containing merely partial shadow areas, it is advisable to set Φ^*_{min} at a small positive value (typically between 0.05 and 0.10).

In principle, the de-shadowing could now be performed with the physically scaled function Φ^*, which represents the fraction of the direct illumination for each pixel in the ρ' vector, i.e., the complete scene without cloud and water pixels. However, since the matched filter is not a perfect shadow transformation, it is much better to restrict its application to the potential, most-likely shadow areas. This is an important processing step to reduce the number of mis-classifications or false-alarms. If omitted it will cause strange 'shadow' pixels scattered all over the image, compare Fig. 2.

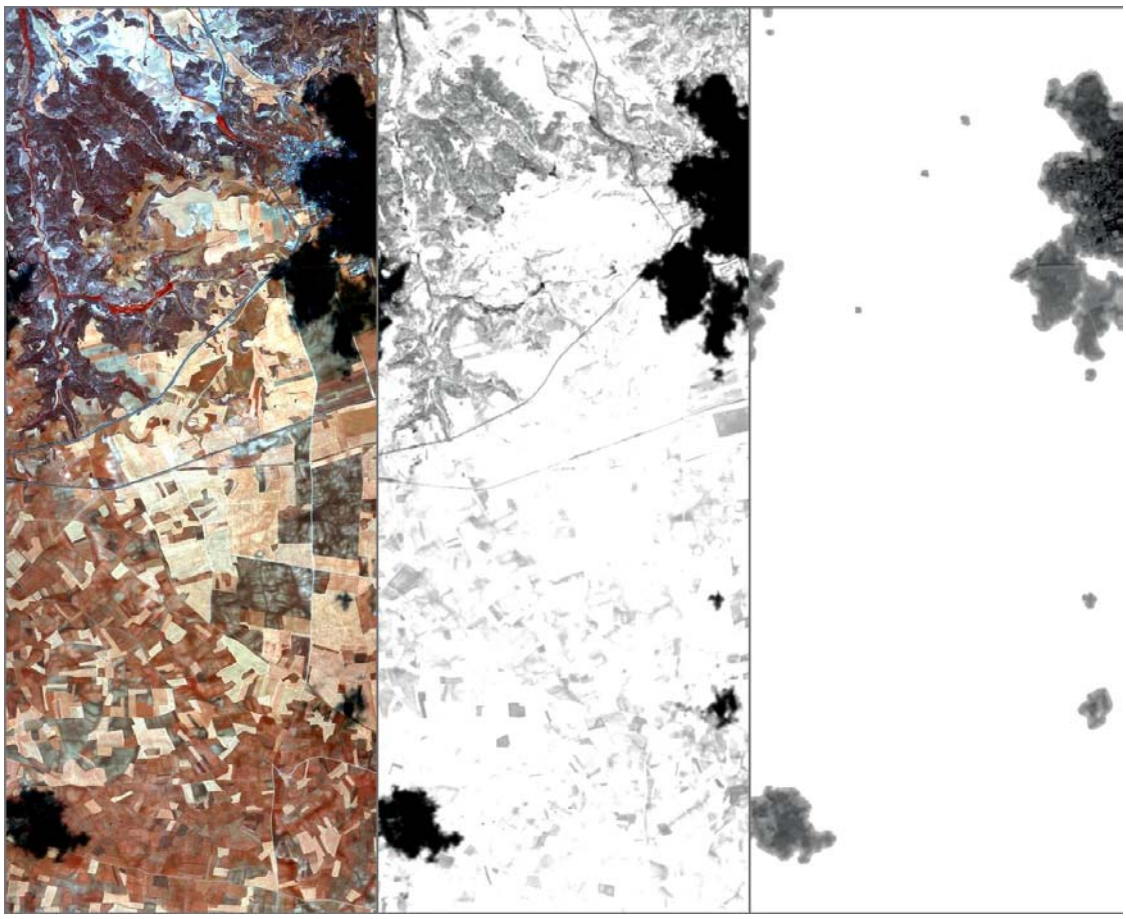

Fig. 2:
Left: surface reflectance image of HyMap at Chinchon, Spain. Colour coding: RGB=878, 646, 462 nm channels.
Center: standard shadow map.
Right: map derived from core shadow regions.

Therefore, the proposed method tries to find the core shadow areas in a scene, and subsequently expands the core regions to obtain the final mask that includes a smooth shadow/clear transition. The physically scaled shadow function Φ^* is then applied only to the pixels in the final mask.

The histogram of the unscaled shadow function Φ can be employed to separate regions of low values of Φ from the moderate-to-high values (see Richter and Müller 2005 for details). A threshold Φ_T can be set in the vicinity of the local histogram minimum and the core shadow mask is defined by those pixels with $\Phi(x,y) < \Phi_T$.

Once the core shadow mask has been defined, it is expanded to include the surrounding shadow/clear transition zone of 100 m width. De-shadowing with the scaled shadow function Φ^* is then exclusively applied to the pixels in this final mask. This means the direct solar flux (E_{dir} term in eq. 1) has to be multiplied with $\Phi^*(x,y)$:

$$\rho_i(x,y) = \frac{\pi\left(d^2\left\{c_0(i)+c_1(i)DN_i(x,y)\right\}-L_{p,i}\right)}{\tau_i\left(E_{dir,i}\;\Phi^*(x,y)+E_{dif,i}\right)} \tag{6}$$

3. EXAMPLES OF DE-SHADOWING IMAGERY

Three selected examples show the performance of the method for a hyperspectral airborne scene and two multispectral satellite scenes.

The first example of processing (Fig. 2, left) demonstrates a successful shadow removal for a situation where all clouds are outside the airborne scene, so a cloud shadow algorithm relying on cloud patterns would fail. The imagery was recorded by the HyMap sensor (Cocks et al. 1998) covering the 0.45 - 2.45 µm spectral region with 126 bands.

Fig. 2 (left) shows the atmospherically corrected surface reflectance image prior to de-shadowing. The center of the figure presents the standard shadow map employing all image pixels. The right part is the corresponding improved shadow map derived from the core shadow areas. Obviously, the standard shadow map contains a lot of misclassified pixels, such as roads, borders between different fields, and others. The improved shadow map also contains some small artifact areas, but it has a much lower number of misclassified pixels. It nicely captures the significant shadow areas. Fig. 3 shows a zoomed view from the top of this scene. It presents reflectance data before de-shadowing, and results after de-shadowing with the core-shadow method.

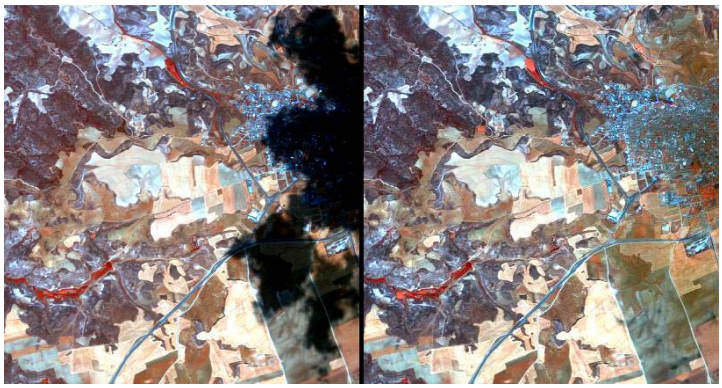

Fig. 3 HyMap scene, 12 July 2003, Chinchon, Spain, RGB = 848, 646, 464 nm

The second sample case presents a subset of a SPOT-5 scene from Rumania, acquired 22 May 2005, containing a large percentage of cloud areas (Fig. 4). A lot of details can be seen in the de-shadowed image that are hidden in the original scene.

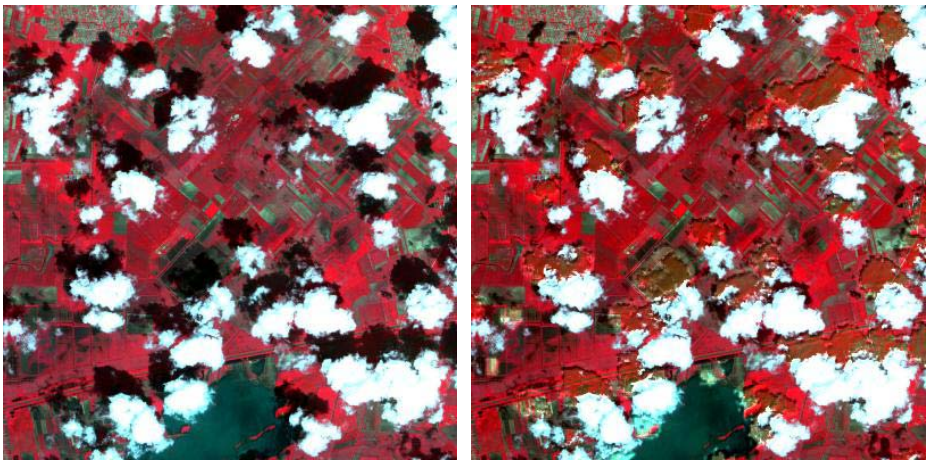

Fig. 4 SPOT-5 scene, RGB=836, 657, 555 nm. Courtesy European Space Imaging.

The third example shows de-shadowing of building shadow areas from a Munich scene recorded by Ikonos, 17 Sept. 2003, see Fig. 5. Although the contrast in the de-shadowed image is drastically reduced as it should be, the zoomed view in shadow areas reveals additional information that cannot be found in the original scene.

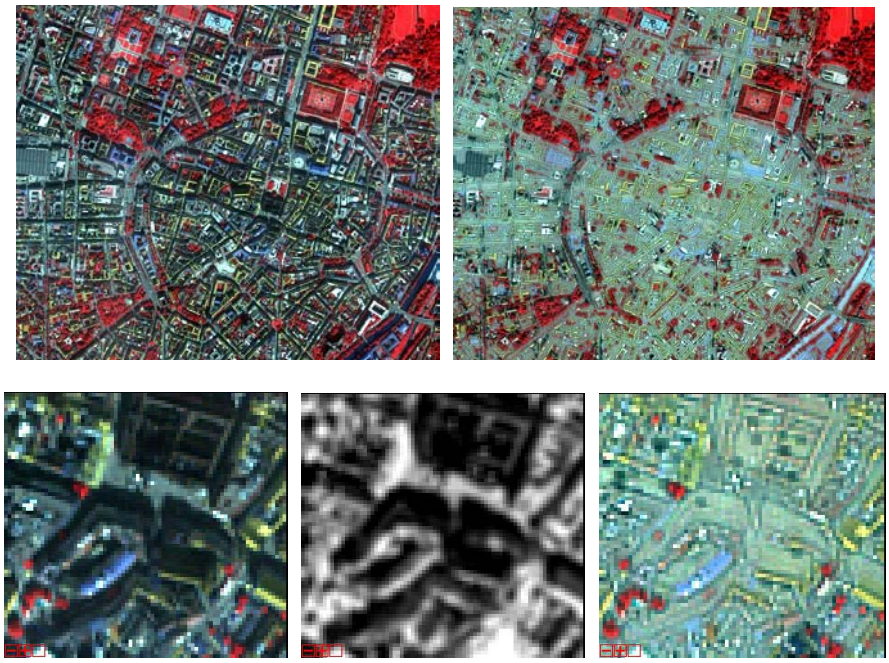

Fig. 5 Ikonos scene of Munich center, RGB=802, 665, 551 nm.
Top left: original, right: after de-shadowing. Courtesy European Space Imaging.
Bottom shows a zoomed view: original, shadow map, de-shadowed image.

4. SUMMARY

A fully automatic de-shadowing method for spectral imagery has been developed. An essential part of the technique is the concept of core shadow and expanded shadow regions to reduce the number of shadow-

pixel misclassifications significantly. The algorithm was implemented with three tunable parameters: the size of the core shadow mask (small, medium, large), the maximum range of the unscaled shadow function, and the minimum fractional direct solar illumination of the darkest shadow areas, the depth of shadow. Once the parameters have been set the algorithm runs fully automatic. Default values are provided that usually yield good de-shadowing results. However, for optimum performance these parameters might have to be tuned depending on the scene.

REFERENCES

Adler-Golden, S.M., Matthew, M. W., Anderson, G. P., Felde, G. W., and Gardner, J. A., 2002, "An algorithm for de-shadowing spectral imagery", *Proc. 11th JPL Airborne Earth Science Workshop, 5-8 March 2002,* JPL-Publication 03-04, Pasadena, U.S.A.

Berk, A., Anderson, G. P., Acharya, P: K., Chetwynd, J. H., Bernstein, L. S., Shettle, E. P., Matthew, M. W., and Adler-Golden, S. M., 2000, "MODTRAN4 User's Manual", Air Force Research Laboratory, Hanscom AFB, MA, U.S.A.

Cocks, T., Jenssen, R., Stewart, A., Wilson, I., and Shields, T., 1998, "The HyMap airborne hyperspectral sensor: the system, calibration and performance", *First EARSeL Workshop on Imaging Spectroscopy, 6-8 Oct. 1998, Zurich, Switzerland*, pp. 37-42.

Richter, R., 1996, "A spatially adaptive fast atmospheric correction algorithm", *Int. J. Remote Sensing,* Vol. 17, 1201-1214.

Richter, R., 1998, "Correction of satellite imagery over mountainous terrain", *Applied Optics,* Vol. 37, 4004-4015.

Richter, R., and Schläpfer, D., 2002, "Geo-atmospheric processing of airborne imaging spectrometry data. Part 2: atmospheric / topographic correction.", *Int. J. Remote Sensing*, Vol. 23, 2631-2649.

Richter, R., and Müller, A., 2005, "De-shadowing of satellite/airborne imagery", accepted for publication, Int. J. Remote Sensing.

Simpson, J. J., and Stitt, J. R., 1998, "A procedure for the detection and removal of cloud shadow from AVHRR data over land", *IEEE Trans. Geoscience and Remote Sensing*, Vol. 36**,** 880-897.